


Article

Experimental Study on Small-Strain Elastic Parameters of Biochar–Methanotroph–Clay Mixture

Shuyun Zhang ¹, Wenjing Sun ^{2,*} , Kun Xu ³ and Deyang Liu ¹

¹ Department of Civil Engineering, School of Mechanics and Engineering Science, Shanghai University, Shanghai 200444, China

² Department of Civil Engineering, College of Environmental Science and Engineering, Donghua University, Shanghai 201600, China

³ Shanghai Dahua Group, Shanghai 200062, China

* Correspondence: wjsun@dhu.edu.cn; Tel.: +86-180-499-63719

Abstract: During the service of a landfill, uneven soil settlement and earthquakes can cause changes to the pore structure and cracks in the covering layer. The use of a biochar–methanotroph–clay mixture as a new landfill covering layer, can improve its engineering properties. The biochar–methanotroph–clay mixture’s shear-wave velocity and compression-wave velocity were measured by the bender–extender element test, and the elastic parameters under small-strain conditions, such as maximum shear modulus, G_{\max} , maximum constrained modulus, M_{\max} , and Poisson’s ratio, ν , were obtained. The parameters showed that the elastic characteristics and lateral deformation capacity were of great significance for settlement, seismic field, and stress–strain analysis. Based on the bender–extender element test, the effects of different compaction degrees, and biochar content on G_{\max} , M_{\max} , and ν of the biochar–clay mixture, and different methane cultivation days on the biochar–methanotroph–clay mixture, were investigated. The results showed that the G_{\max} , M_{\max} , and ν of the biochar–clay mixture increased with the increase in biochar content and dry density. When the biochar content was 15%, and the dry density was 1.64 g/cm^3 , the ν increased significantly. The G_{\max} and M_{\max} of the biochar–methanotroph–clay mixture tended to increase with the increase in methane cultivation days, and the higher the biochar content, the more obvious the increasing trend. The ν showed a decreasing trend with the increase in methane cultivation days, and the resistance to lateral deformation was stronger.

Keywords: biochar–methanotroph–clay mixture; bender–extender elements; maximum shear modulus; maximum constrained modulus; Poisson’s ratio



Citation: Zhang, S.; Sun, W.; Xu, K.; Liu, D. Experimental Study on Small-Strain Elastic Parameters of Biochar–Methanotroph–Clay Mixture. *Processes* **2023**, *11*, 982. <https://doi.org/10.3390/pr11040982>

Academic Editors: Kassio Ferreira Mendes and Renata Pereira Lopes

Received: 21 February 2023
Revised: 17 March 2023
Accepted: 19 March 2023
Published: 23 March 2023



Copyright: © 2023 by the authors. Licensee MDPI, Basel, Switzerland. This article is an open access article distributed under the terms and conditions of the Creative Commons Attribution (CC BY) license (<https://creativecommons.org/licenses/by/4.0/>).

1. Introduction

With increasing urbanization, domestic waste output has increased and threatened the environment. Waste disposal methods include sanitary landfill, mixed composting, and incineration [1]. The sanitary landfill method is widely used, due to its low cost and ease of implementation. During the service of the landfill, harmful gases (such as methane, carbon dioxide, hydrogen sulfide gas, etc.) will be released, among which, methane has 28 times the greenhouse potential of carbon dioxide [2]. In old landfills, methane escapes, due to a lack of complete gas collection devices, which is prone to explosion and collapse once the concentration reaches a critical value. Therefore, an economical and sustainable technology for the landfill covering layer is needed, to reduce the emission of methane [3]. The use of compacted clay as a covering layer is a common treatment method, but is inefficient for methane removal. The incorporation of biochar and methanotrophs can improve the efficiency of methane removal. Biochar is a material with loose porous properties and has an adsorption effect on methane [4]. Methanotrophs are microorganisms that use methane as their only carbon source and can oxidize methane, and the oxidation equation is as Equation (1). Biochar can provide a beneficial condition for methanotrophs, to enhance

methane oxidation efficiency [5,6]. $R = (C_0 - C_f)/C_0 \times 100\%$ is used to calculate the methane removal rate, where C_0 and C_f are the initial and final methane concentrations (%), respectively. Meanwhile, it was found that incorporating biochar and methanotrophs could improve the soil structure and enhance the soil integrity [7–9]. Therefore, the biochar–methanotroph–clay mixture covering layer was used as a new covering layer, as shown in Figure 1.

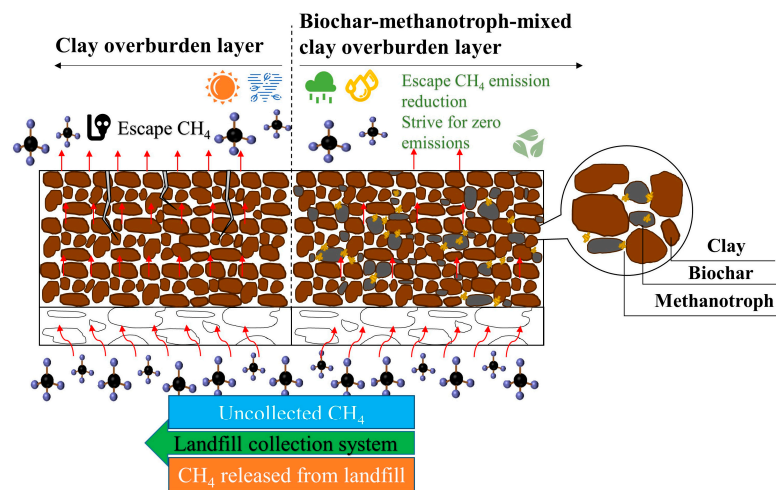
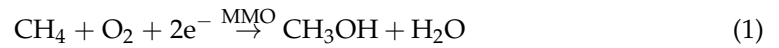


Figure 1. Schematic diagram of biochar–methanotroph–clay covering layer.

However, uneven soil settlement and earthquakes lead to changes in pore structure and cracks of the covering layer, weakening the integrity of the covering layer and affecting the engineering properties, such as the small-strain elastic parameters [10]. The elastic parameters such as shear modulus, G , constrained modulus, M and Poisson's ratio, ν , are important parameters in the engineering properties of the covering layer, and are of great significance for the seismic field, settlement, and stress–strain analysis [11]. Therefore, it is necessary to study these parameters. Among them, shear modulus, G , and constrained modulus, M , reflect the elastic properties of the covering layer [12,13], and Poisson's ratio, ν , reflects the lateral deformation. The bender–extender test can obtain these parameters. In 1978, Shirley et al. [14] obtained the small-strain shear modulus using the bender elements, which is a low-cost and nondestructive method. The growth of methanotrophs is irreversible, the bender–extender test has less influence on methanotrophs [15]. Therefore, the small-strain elastic parameters of the biochar–methanotroph–clay mixture covering layer, can be studied by bender–extender elements [16–18].

Different factors affect the elastic parameters of the soil under small-strain conditions. Scholars have studied common factors such as dry density, admixture, and microbial growth. Gu et al. [19] studied the effect of compaction degree on the shear modulus, G_0 , constrained modulus, M_0 , and Poisson's ratio, ν , of sandy soil, by a bender–extender element test, and found that as the compaction degree increased, the ν decreased, and the G_0 and M_0 increased. Głuchowski et al. [20] measured the shear modulus G_0 of sandy silt, by triaxial tests with bender elements, and found that the G_0 increased with the increase in compaction degree. Liu et al. [21] studied the influence of sand content in loess on compression-wave (P-wave) velocity, V_p , and shear-wave (S-wave) velocity, V_s , by a triaxial device with a bender–extender element, and found that V_p and V_s decreased with the increase in sand content. Ruan et al. [22] studied the effect of fine grain content on the maximum shear modulus, G_{\max} , of saturated sand by the bender element, and found that the G_{\max} decreased first and then increased, with the increase in fine grain content. Gao et al. [23], measured the shear-wave modulus of bacteria-doped clay with a piezo-ceramic device, and found that at 25 °C, the number of *Streptomyces* increased. The extracellular

polysaccharides can fill pores in between the particles and increase the shear modulus. The above research focused on the maximum shear modulus, G_{\max} , of different types of soils, while few studies had been conducted on the G_{\max} , maximum constrained modulus, M_{\max} , and Poisson's ratio, ν , of biochar–methanotroph–clay mixtures. The effect of the growth of methanotrophs on the covering layer is considered here, to study the long-term use stability. The effects of dry density, biochar content, and methanotroph growth on the elastic parameters under small-strain conditions should be studied. This provides a reference for forming an optimal covering layer design scheme with these materials in the actual landfill, and also simulates the deformability characteristics of the covering layer after long-term use.

This study selected biochar, methanotrophs, and clay as the covering layer materials, for improving engineering properties. The maximum shear-wave velocity and maximum constrained wave velocity of the biochar–methanotroph–clay mixture, were measured by the bender–extender elements, and the maximum shear modulus, G_{\max} , maximum constrained modulus, M_{\max} , and Poisson's ratio, ν , were calculated. The effects of different compaction degrees and biochar content on the G_{\max} , M_{\max} , and ν of the non-methanotroph-doped clay, and different methane cultivation days on methanotroph-doped clay, were investigated to provide a reference for the design of a biochar–methanotroph–clay mixture covering layer, instead of a traditional clay covering layer.

2. Materials and Methods

2.1. Materials

The main materials used in this experiment were clay, biochar, and methanotrophs. The clay was the fourth layer of Shanghai muddy clay, from a construction site in Yangpu, Shanghai. The clay properties were obtained according to the standard for soil test method (GB 50123) [24]. The specific gravity of the clay and biochar was obtained by the gravimetric method. The plastic limit and liquid limit were measured using the liquid–plastic limit combined test, to calculate the plastic index. The maximum dry density and optimum moisture content of the clay were obtained by the light compaction test. The ash and pH of the biochar were measured according to the standard test method [25]. The main physical indexes of the clay are shown in Table 1. The biochar was produced by Desheng Company in Liyang, and the raw material was rice straw, which was obtained by pyrolysis, under anoxic conditions, at 500 °C. The main physical indexes are shown in Table 2. The pH of the biochar was 7.70, the pH of the biochar–clay mixture with 10% biochar content was 8.00, and the biochar–clay mixture with 15% biochar content was 8.30. The proximate and ultimate compositions of the biochar are shown in Table 3.

Table 1. Main physical indexes of clay.

Specific Gravity G_s	Liquid Limit $w_L/\%$	Plastic Limit $w_P/\%$	Plasticity Index I_P	Maximum Dry Density $\rho_{d\max}/(\text{g}/\text{cm}^3)$	Optimum Moisture Content $w_{\text{opt}}/\%$
2.71	42.04	24.00	18.04	1.63	22.00

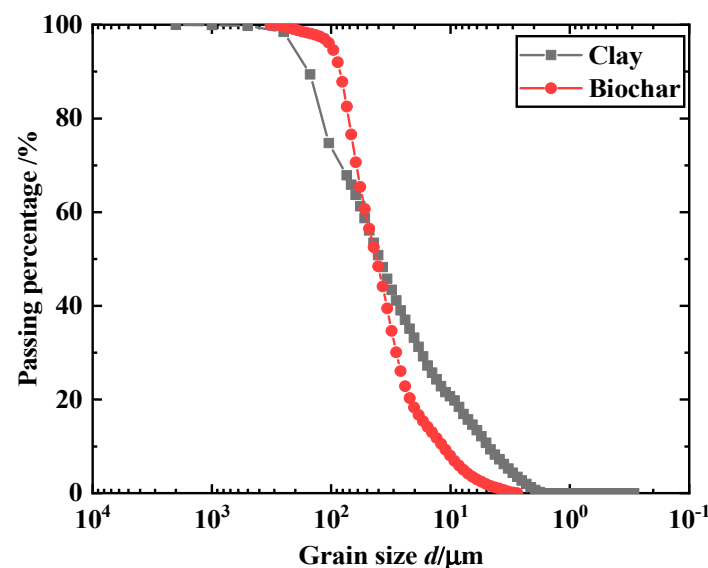
Table 2. Main physical indexes of biochar.

Specific Surface Area (m^2/g)	Specific Gravity G_s	Bulk Density $\rho_b/(\text{g}/\text{cm}^3)$	pH
385.60	1.99	0.55	7.70

Table 3. Proximate and ultimate composition analysis of biochar.

Proximate Composition/%			Ultimate Composition/%			
Ash Content	Volatile Matter	Fixed Carbon	C	O	N	S
18.80	66.11	15.09	50.46	48.74	0.80	0.00

Figure 2 shows the grain-size distributions of the clay and biochar. The particle size $> 74 \mu\text{m}$ was measured by the sieving method, and the particle size $< 74 \mu\text{m}$ was measured by a laser granularity analyzer. The liquid–plastic limit and plastic index determined the clay to be a low-liquid limit clay (CL). The clay was identified as a low-liquid limit clay (CL) based on its liquid limit, plastic limit, and plasticity index. According to the grain-size distribution, the clay contained 32.14% sand grains, 57.11% fines, and 10.75% clay grains.

**Figure 2.** Grain-size distributions of the clay and biochar.

The soil from the Shanghai Laogang landfill covering layer was mixed with deionized water, to separate the bacteria from the soil and dissolve the bacteria in the water. The supernatant was taken after shaking, to prepare the inorganic salt culture solution for screening for methanotrophs. The components of the inorganic salt cultures were, $\text{MgSO}_4 \cdot 7\text{H}_2\text{O}$ (1.0 g), KNO_3 (1.0 g), $\text{Na}_2\text{HPO}_4 \cdot 2\text{H}_2\text{O}$ (0.717 g), KH_2PO_4 (0.272 g), NH_4Cl (0.25 g), Anhydrous CaCl_2 (0.1 g), FeCl_3 (0.004 g), $\text{Na}_2\text{-DTA}$ (0.5 g), $\text{FeSO}_4 \cdot 7\text{H}_2\text{O}$ (0.2 g), $\text{MnSO}_4 \cdot \text{H}_2\text{O}$ (0.003 g), $\text{CuSO}_4 \cdot 7\text{H}_2\text{O}$ (0.03 g), $\text{ZnSO}_4 \cdot 7\text{H}_2\text{O}$ (0.01 g), $\text{NaMoO}_4 \cdot 2\text{H}_2\text{O}$ (0.003 g), $\text{NiCl}_2 \cdot 6\text{H}_2\text{O}$ (0.01 g), $\text{CoCl}_2 \cdot 6\text{H}_2\text{O}$ (0.048 g), H_3BO_3 (0.062 g). After that, the supernatant and inorganic salt culture solution were mixed, at a ratio of 1:50, in a serum bottle and filled with methane. A Luria–Bertani (LB) solid medium was prepared. After cooling and solidification, a sterilization inoculation ring was dipped into the bacterial solution and streaked on the LB medium, which is the streaking step. Agar powder (10 g), 10 g of peptone, 5 g of yeast powder, and 10 g of NaCl were mixed with deionized water and diluted to 1 L, in a constant volume flask, to make Luria–Bertani (LB) culture solution, and the screened methanotrophs were poured into the LB culture solution and shaken in an oscillator for three days, to obtain the methanotroph solution. After DNA identification, the screened bacterium was *methylobacterium extorquens*, a kind of aerobic methanotroph belonging to type I, γ -Proteobacteria, *Methylobacter* [26]. The appearance of the methanotrophs was rod-shaped, as shown in Figure 3, determined using an XSP-2CA biomicroscope.

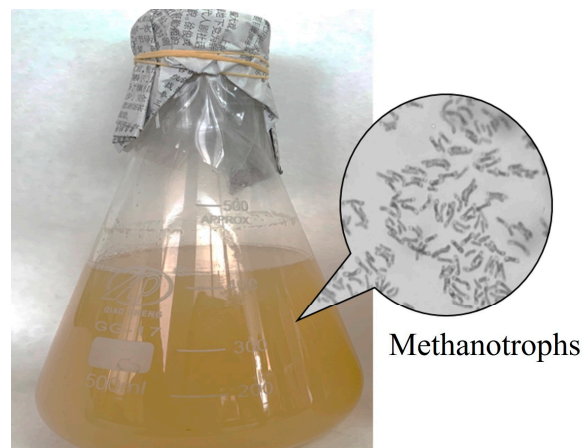


Figure 3. Methanotroph solution and morphology.

2.2. Apparatus

The apparatus used was the bender–extender element, GDS, UK, a device that converts mechanical and electrical signals, using piezoelectric and inverse piezoelectric effects of piezoelectric ceramic materials [27]. Figure 4 shows the bender–extender element system, which can conduct S-wave (shear wave) and P-wave (compression wave) tests. The device has a Y-shaped piezoelectric ceramic piece at the top, as the S-wave transmitter and P-wave receiver, and an X-shaped piezoelectric ceramic piece at the bottom, as the S-wave receiver and P-wave transmitter. In the test, an appropriate emission frequency is selected, to emit a sine wave, and the time domain initial wave method is used to obtain the reproduction time of each wave. For the S-wave, a voltage pulse of emission signals is applied to the top of the bending element. The piezoelectric ceramic piece with the same polarization direction, forms a lateral vibration and passes through the soil sample until the S-wave reaches the bottom, where it receives the S-wave and converts it into an electrical signal, that is displayed and stored on the oscilloscope. The shear-wave reproduction time t_s is obtained. For the P-wave, a voltage pulse of emission signals is applied to the bottom, and the piezoelectric ceramic piece with the opposite polarization direction will be elongated or shortened, to form a vertical vibration, which is transmitted in the soil sample until the P-wave is transmitted to the top, where it receives the P-wave and transforms it into an electrical signal. The compressional wave reproduction time, t_p , is obtained. The shear-wave velocity, V_s , and compression-wave velocity, V_p , can be calculated from the reproduction distance, L , according to Equations (2) and (3).

$$V_s = \frac{L}{t_s} \quad (2)$$

$$V_p = \frac{L}{t_p} \quad (3)$$

where L is the height of the specimen (mm); t_s is the reproduction time of the shear wave(s); and t_p is the reproduction time of the compressional wave (s).

From the shear-wave velocity, V_s , and compression-wave velocity, V_p , measured by the bender–extender element system, the maximum shear modulus, G_{\max} , and the constrained modulus, M_{\max} , can be calculated according to Equations (4) and (5) [28].

$$G_{\max} = \rho V_s^2 \quad (4)$$

$$M_{\max} = \rho V_p^2 \quad (5)$$

where G_{\max} is the maximum shear modulus (MPa), M_{\max} is the maximum constrained modulus (MPa), and ρ is the density (g/cm^3).

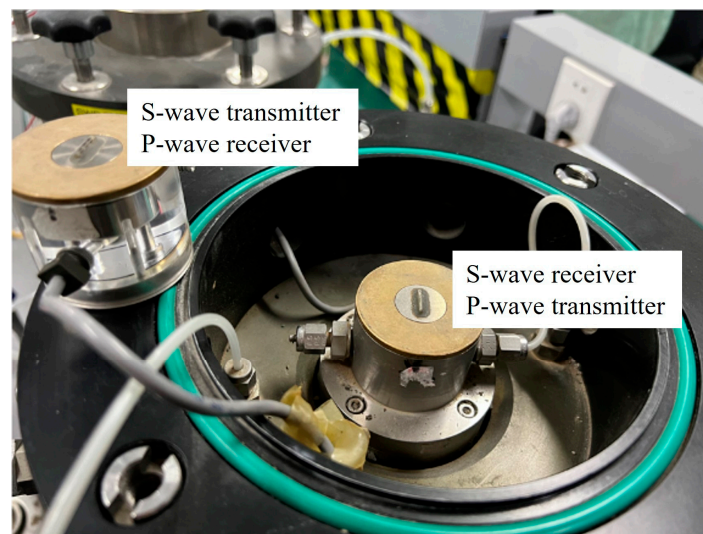


Figure 4. Bender–extender element system.

From the maximum shear modulus, G_{\max} , and the maximum constrained modulus, M_{\max} , of the soil, the Poisson's ratio ν of the soil can be calculated by Equation (6) [28].

$$\nu = \frac{2G_{\max} - M_{\max}}{2(G_{\max} - M_{\max})} \quad (6)$$

where ν is the Poisson's ratio.

2.3. Test Method

The effects of biochar content, dry density, and methane cultivation days on the maximum shear modulus, G_{\max} , and maximum constrained modulus, M_{\max} , of the biochar–methanotroph–clay mixture, were investigated. Based on the optimum moisture content of clay [29], the initial moisture content of the non-methanotroph-doped group was 22%, the dry density was 1.48 g/cm³, 1.56 g/cm³, and 1.64 g/cm³, and the biochar content was 0, 10, and 15%. The initial bacterial liquid content rate (the ratio of the mass of bacterial liquid in the soil to the mass of dry soil) of the methanotroph-doped group was 22%, which is the same as the control variables of the non-methanotroph-doped group. The saturation was 70–90%, the presence of pores can accommodate methane, to supply the growth and reproduction of methanotrophs. The dry density and biochar content were the same as above. The methanotroph solution was mixed with biochar and clay. The mixture was put into the sample-making mold, with a diameter of 5 cm and a height of 5 cm, then compacted at a certain dry density. The samples were put into the incubator, the air was pumped out with a syringe, and the methane was filled to a concentration of 3%. A portable methane detector measured the methane concentration in the incubator every day. If the detected methane concentration decreased, the incubator was refilled with methane, to keep the detected methane concentration stable at 3%. The samples were incubated for 0, 10, 20, and 30 days and then taken out for the bender element test at the specified methane cultivation day. Nine samples were produced for the sterile and bacterial groups, and plastic molds were printed using 3D scanning technology. The molds were used to press grooves at the upper and lower ends of the soil sample, to fit better with the bender element crystal and make the test results accurate, as shown in Figure 5. The samples were placed on the base and the upper receiver was installed, during the bender–extender element test. The bender–extender element was turned on, and the shear or compression wave was emitted. The reproduction velocity of the shear or compression wave in the soil was obtained after the signal processor, and the maximum shear, constrained modulus, and Poisson's ratio were calculated.

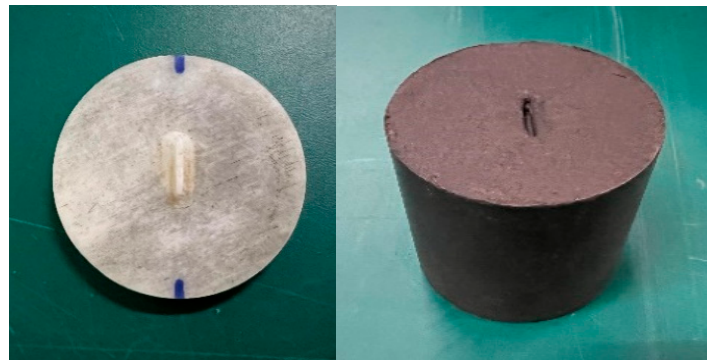


Figure 5. Plastic mold and biochar–methanotroph–clay mixture compaction sample.

3. Results

3.1. Maximum Shear Modulus, Maximum Constrained Modulus, and Poisson's Ratio of the Biochar–Clay Mixture

Figure 6 shows the relationship between the maximum shear modulus, G_{\max} , maximum constrained modulus, M_{\max} , and dry density ρ_d of the biochar–clay mixture. Figure 6a shows the relationship between G_{\max} and ρ_d . It was found that, under the same biochar content, the G_{\max} increased with the increase in dry density, that is, compaction degree. Figure 6b shows the relationship between M_{\max} and ρ_d , and it was found that under the same biochar content, the M_{\max} increased with the increase in dry density. When the biochar content was 10 and 15%, that is, after the incorporation of biochar, the constrained modulus, M_{\max} , increased obviously, with an increase in dry density. G_{\max} and M_{\max} are important parameters of soil stiffness [30], which reflect the deformation capacity. The higher the compaction degree, the smaller the void ratio, the closer the contact between particles, the stronger the cementation capacity, the more stable the soil structure, and the stronger the resistance to deformation [31].

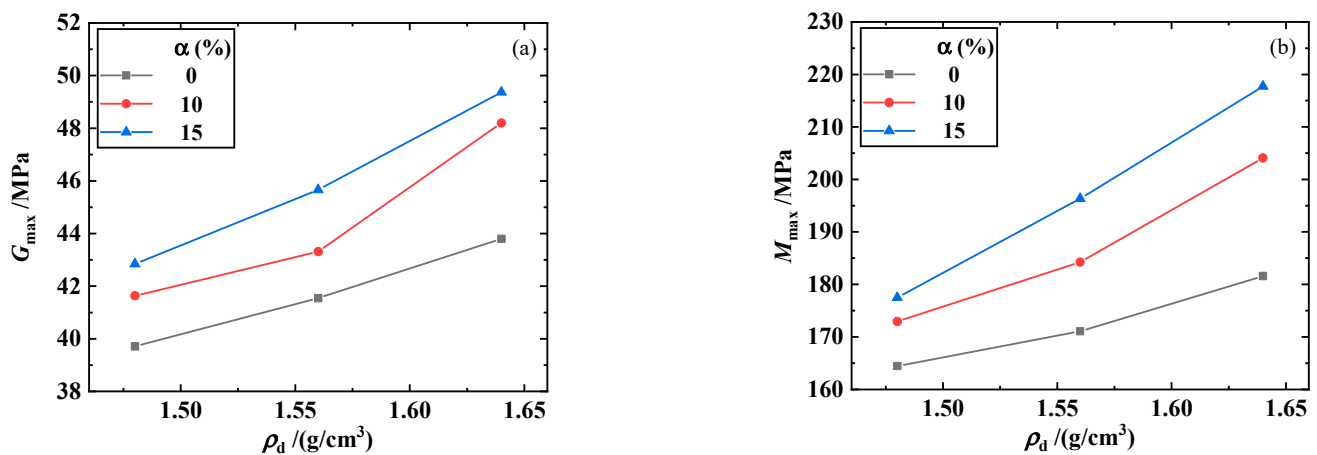


Figure 6. Relationship between G_{\max} , M_{\max} , and dry density, ρ_d , of the biochar–clay mixture: (a) G_{\max} – ρ_d ; (b) M_{\max} – ρ_d .

The Poisson's ratio, ν , was calculated from G_{\max} and M_{\max} , according to Equation (6). Figure 7 shows the variation in Poisson's ratio of the biochar–clay mixture with dry density, under different biochar content, from which it can be seen that, when the biochar content was 0% (pure clay), the Poisson's ratio did not change significantly with the increase in dry density. When the biochar content was 10%, the Poisson's ratio first increased and then tended to remain stable with the increase in dry density. When the biochar content was 15%, the Poisson's ratio of the biochar–clay mixture showed an increasing trend with the increase in dry density. The Poisson's ratio of soil, is the ratio of normal transverse strain to

normal axial strain, which is the elastic constant reflecting the transverse deformation of the material [21]. As the dry density increases, the void ratio decreases, and the pore gas volume in the three-phase composition of the soil is compressed, so the transverse strain increases and the volume strain decreases under a certain axial strain in the small-strain state [32], and the Poisson's ratio increases.

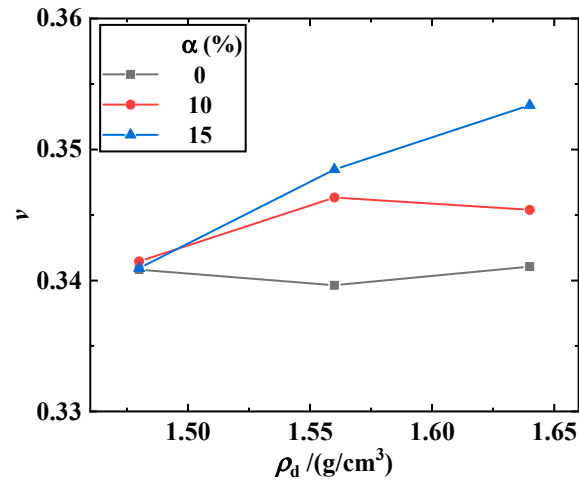


Figure 7. Relationship between Poisson's ratio and dry density of the biochar-clay mixture.

Figure 8 shows the relationship between the maximum shear modulus, G_{\max} , the maximum constrained modulus, M_{\max} , and the biochar content, α , of the biochar-clay mixture. Figure 8a shows the relationship between G_{\max} and α . It is found that, under the same dry density, G_{\max} increases with the increase in biochar content. When the dry density was 1.48 g/cm^3 and 1.56 g/cm^3 , G_{\max} increased slightly with the increase in biochar content. Figure 8b is the relationship between M_{\max} and α . It was found that under the same dry density, the M_{\max} increased with the increase in biochar content, and when the dry density was 1.64 g/cm^3 , M_{\max} increased most obviously. The fine particles of biochar fill the intergranular pores of the mixture, the number of intergranular pores and macropores is reduced, the cohesion between particles is generated, the soil structure is stable, and the resistance to deformation is enhanced.

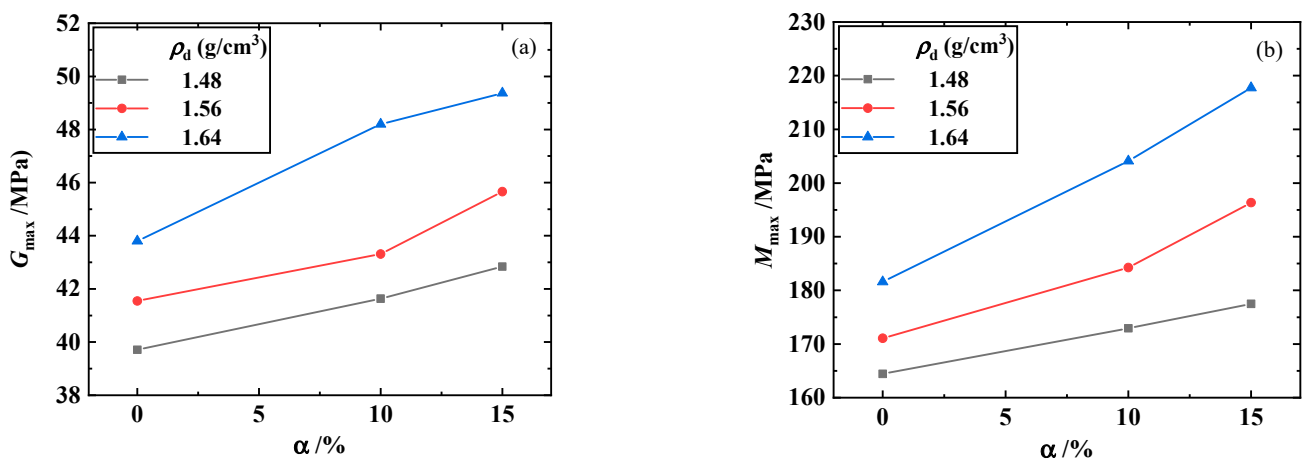


Figure 8. Relationship between G_{\max} , M_{\max} , and biochar content α of the biochar-clay mixture: (a) G_{\max} - α ; (b) M_{\max} - α .

Figure 9 shows the relationship between the Poisson's ratio and the biochar content of the biochar-clay mixture. It can be found that the Poisson's ratio tended to change little with the increase in biochar content when the dry density was 1.48 g/cm^3 , but increased

significantly when the dry density was 1.56 g/cm^3 and 1.64 g/cm^3 . The greater the dry density, the more obviously the Poisson's ratio increases. Within the same dry density variation range, the higher the biochar content, the more obvious the increasing trend of Poisson's ratio. With the increase in biochar content, the small particles of biochar fill the pores between the clay aggregates, the void ratio decreases, and the pore gas volume in the three-phase composition of soil compresses, so that the axial strain remains unchanged under the small-strain condition; the transverse strain increases, the volume strain decreases, and the Poisson's ratio increases.

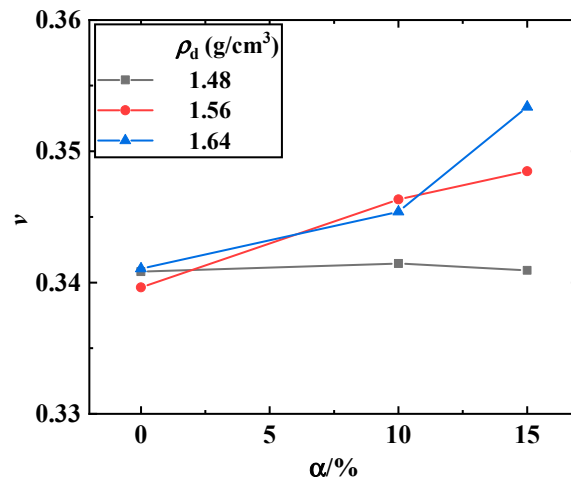


Figure 9. Relationship between Poisson's ratio and biochar content of the biochar–clay mixture.

3.2. Maximum Shear Modulus, Maximum Constrained Modulus, and Poisson's Ratio of the Biochar–Methanotroph–Clay Mixture

Figure 10 compares the G_{max} and M_{max} of the biochar–clay mixture. The biochar–methanotroph–clay mixture had a bacterial liquid content of 22%, and the binder–extender element test was conducted immediately after the sample is made. The results of the methanotroph-doped clay were similar to the non-methanotroph-doped clay, and the methanotrophs did not have a sufficient opportunity to grow and reproduce at this time, indicating the accuracy of the test. This is the basis for studying the variation in G_{max} , M_{max} , and ν of the biochar–methanotroph–clay mixture with methane cultivation days.

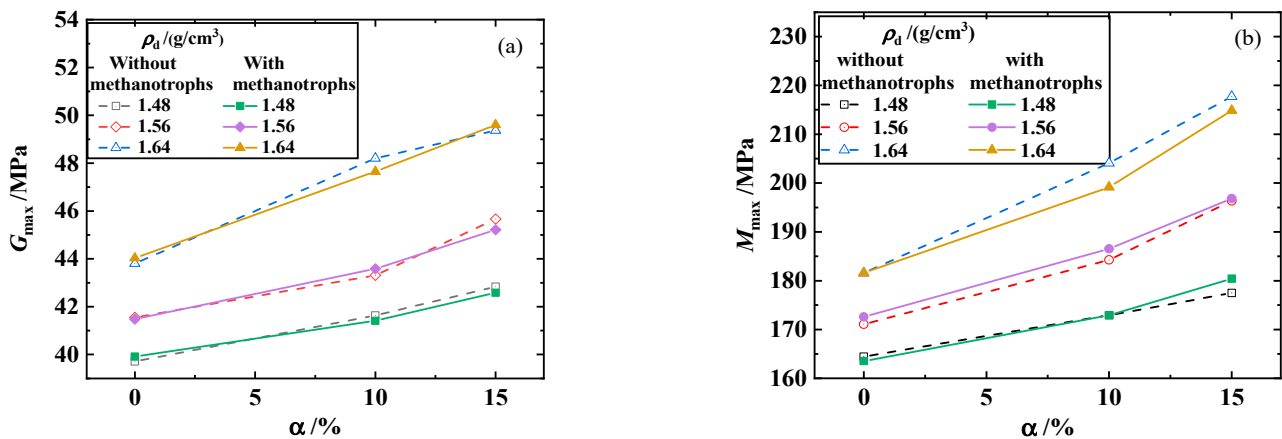


Figure 10. Comparison of G_{max} and M_{max} of the biochar–clay mixture with or without methanotrophs: (a) $G_{max}-\alpha$; (b) $M_{max}-\alpha$.

Figure 11 shows the relationship between maximum shear modulus, G_{max} , and methane cultivation days of the biochar–methanotroph–clay mixture, under different biochar contents. Figure 11a shows the relationship between G_{max} and methane cultivation

days ($\alpha = 0\%$), and the G_{\max} increases slightly with the increase in methane cultivation days. Since pure clay tends to form agglomerates between particles, tight bonding closes the pores leading to the outside, reducing the oxygen content required for the growth of methanotrophs. Hence, their reproduction and activity are limited. Figure 11b shows the G_{\max} and methane cultivation days ($\alpha = 10\%$), it is found that the maximum shear modulus increases with the increase in methane cultivation days, and the trend is relatively gentle. Figure 11c shows G_{\max} and methane cultivation days ($\alpha = 15\%$); it was found that under small dry density, the G_{\max} increased with the increase in methane cultivation days, from 42.6 MPa to 47.2 MPa, an increase of about 11%, which is obvious. When the dry density was high, the G_{\max} remained stable between 0 and 10 days, but increased significantly between 10 and 30 days. The higher the biochar content, the more obvious the increasing trend. Because, after the incorporation of biochar, the porous structure provides space for the growth and reproduction of methanotrophs. The strains, hyphae, and biological flocculation substances, such as proteins or polysaccharides, produced during growth and reproduction, can fill the pores between the aggregates and effectively connect the soil particles, making the soil structure stable and the deformation resistance strong [33].

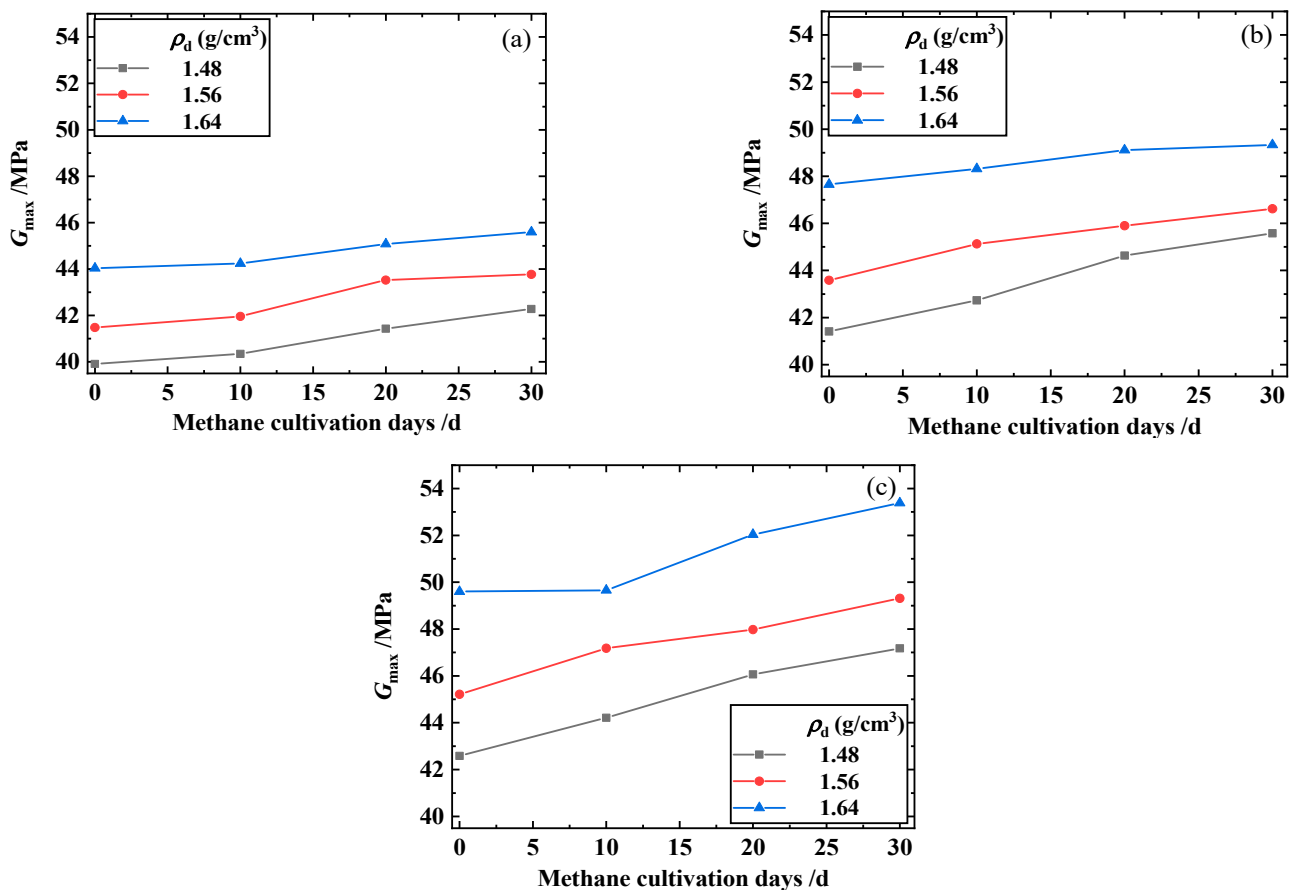


Figure 11. Relationship between G_{\max} and methane cultivation days of the biochar–methanotroph–clay mixture, under different biochar contents: (a) $\alpha = 0\%$; (b) $\alpha = 10\%$; (c) $\alpha = 15\%$.

Figure 12 shows the relationship between the maximum constrained modulus, M_{\max} , and methane cultivation days of the biochar–methanotroph–clay mixture under different biochar contents. It was found that, when the dry density and the biochar content were the same, the maximum constrained modulus, M_{\max} , increased with the increase in methane cultivation days, but the trend was gentle. The methane cultivation days had little effect on the maximum constrained modulus, M_{\max} . When the dry density was large, the maximum constrained modulus, M_{\max} , of the mixture increased, because the void ratio decreased,

and the soil structure became more stable. When the biochar content increases, the pores between the large particles are filled with biochar particles, the number of pores decreases, and the resistance to deformation is enhanced, so the maximum constrained modulus, M_{\max} , increases.

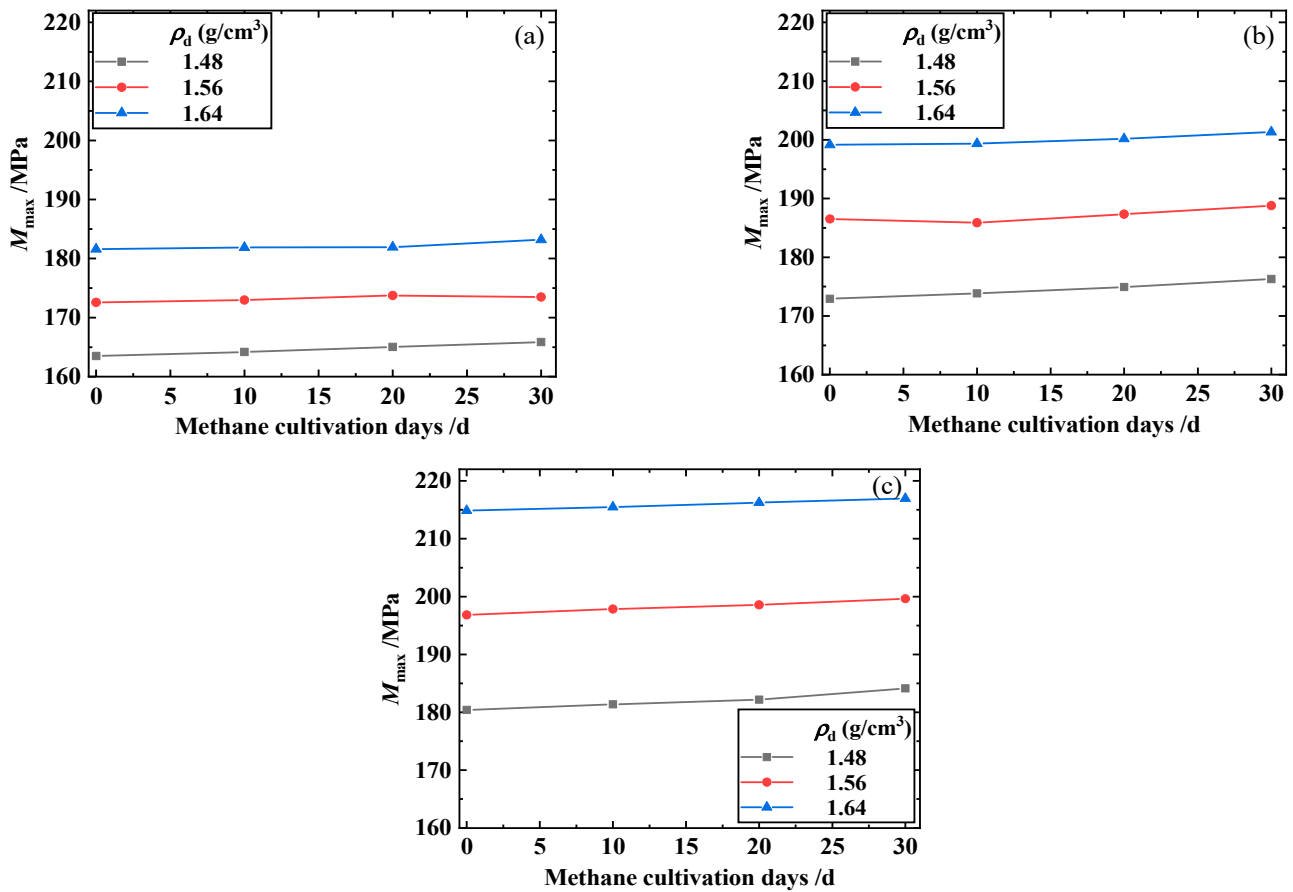


Figure 12. Relationship between M_{\max} and methane cultivation days of the biochar–methanotroph–clay mixture, under different biochar contents: (a) $\alpha = 0\%$; (b) $\alpha = 10\%$; (c) $\alpha = 15\%$.

Figure 13 shows the relationship between Poisson’s ratio and methane cultivation days of the biochar–methanotroph–clay mixture, under different biochar contents. Figure 13a shows that the Poisson’s ratio decreased with the increase in methane cultivation days when the biochar content was 0%, that is, pure clay, and the trend was small in the first ten days and obvious from 10 to 30 days. In Figure 13b, the Poisson’s ratio decreased with the increase in methane cultivation days when the biochar content was 10%. The decreasing trend was obvious in the first ten days and small from 10 to 30 days. In Figure 13c, the Poisson’s ratio decreased significantly with the increase in methane cultivation days when the biochar content was 15%. Biochar is loose and porous, and the incorporation of biochar can improve the characteristics of clay, which has a dense layer and poor air permeability, due to high clay content. Methanotrophs are microorganisms that use methane as the sole carbon source, and the pores of the mixture increase after the incorporation of biochar, which provides methanotrophs with methane and oxygen entry channels and the growth space required for reproduction. Due to the incorporation of biochar, the methanotrophs grow and reproduce faster in clay, producing a large amount of extracellular polymeric substances (EPS). These substances can fill the pores between the clays [18], making the soil structure stable and the lateral deformation small, so the Poisson’s ratio is smaller. The activity of methanotrophs decreases with the increase in methane cultivation days, and the Poisson’s ratio tends to decrease.

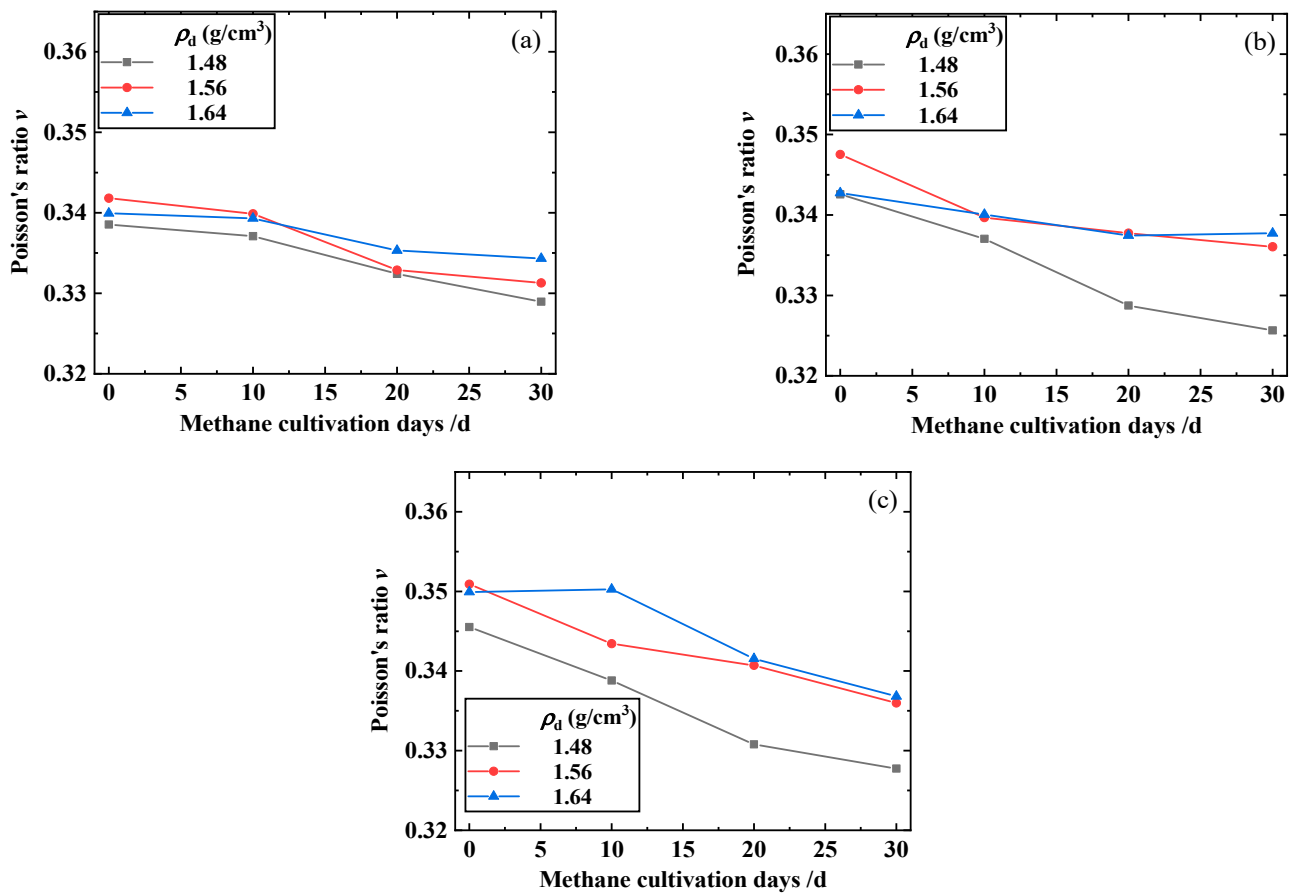


Figure 13. Relationship between Poisson's ratio and methane cultivation days of the biochar–methanotroph–clay mixture, under different biochar contents: (a) $\alpha = 0\%$; (b) $\alpha = 10\%$; (c) $\alpha = 15\%$.

4. Discussion

The maximum shear modulus, G_{\max} , maximum constrained modulus, M_{\max} , and Poisson's ratio, ν , of the biochar–clay mixture, increase with the increase in the dry density. Scanning electron microscopy (SEM) was used to analyze the mixture's microscopic structure. The BET test was used to measure the specific surface area. The SEM images and BET results of the biochar–clay mixture with different dry densities are shown in Figures 14 and 15. When the dry density is 1.48 g/cm^3 , there are more pores between the biochar–clay mixture, mainly large pores between clay aggregates, inter-skeletal pores formed by the contact between biochar particles and clay, and small pores between biochar particles, due to the biochar's loose porosity. When the dry density is 1.64 g/cm^3 , the quantity of pores decreases, with less tightly connected particle voids and a dense structure. As shown in Figure 15, the overall pore-specific surface area decreases with the increase in dry density, the pore volume is compressed. The soil's porosity decreases, and the soil's structure becomes more stable, increasing the resistance capacity to deformation.

The maximum shear, constrained modulus, and Poisson's ratio of the biochar–clay mixture, increase with the increase in biochar content. Figure 16 shows the SEM images of the biochar–clay mixture with different biochar contents. It is found that at a biochar content of 10%, the quantity of pores in the compacted soil is large. Still, at a biochar content of 15%, the pore structure is partially filled by biochar, the quantity of pores decreases and the structure becomes compact. Li et al. [34] found many inter-agglomerate pores in the clay. Still, with the increase in biochar content, the particles filled the pores between the clay particles, so soil particles were arranged more closely, and the quantity of inter-agglomerate and large pores decreased. The soil became dense, and the deformation occurred less.

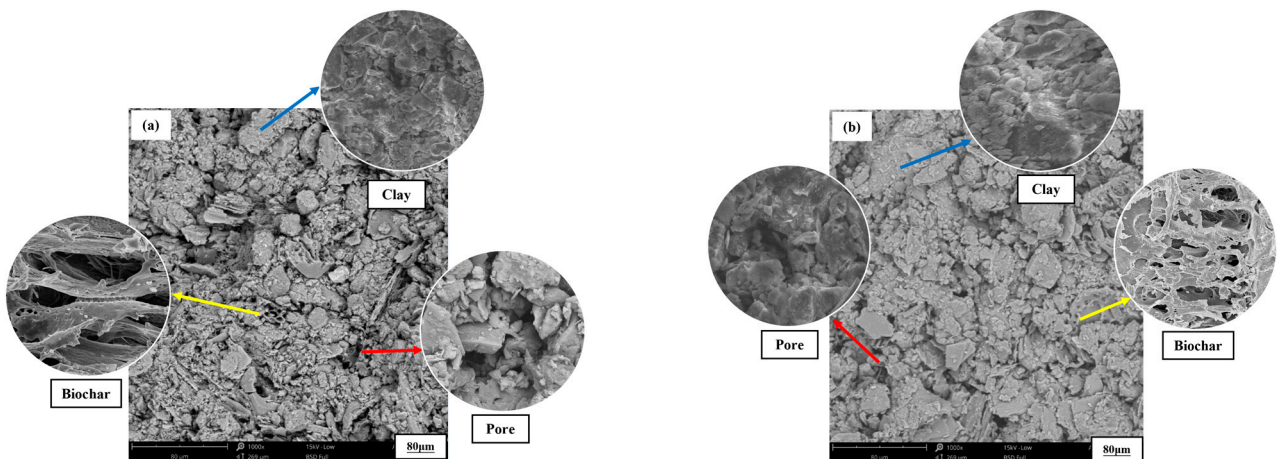


Figure 14. SEM images of the biochar–clay mixture under different dry densities: (a) $\rho_d = 1.48 \text{ g/cm}^3$; (b) $\rho_d = 1.64 \text{ g/cm}^3$.

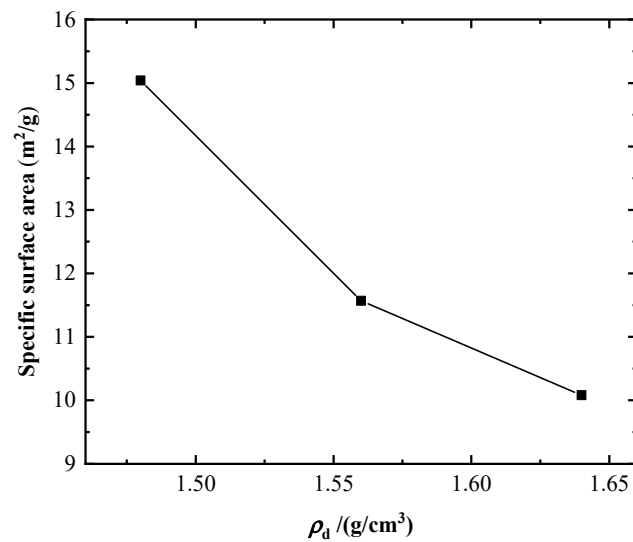


Figure 15. The specific surface area of the biochar–clay mixture under different dry densities.

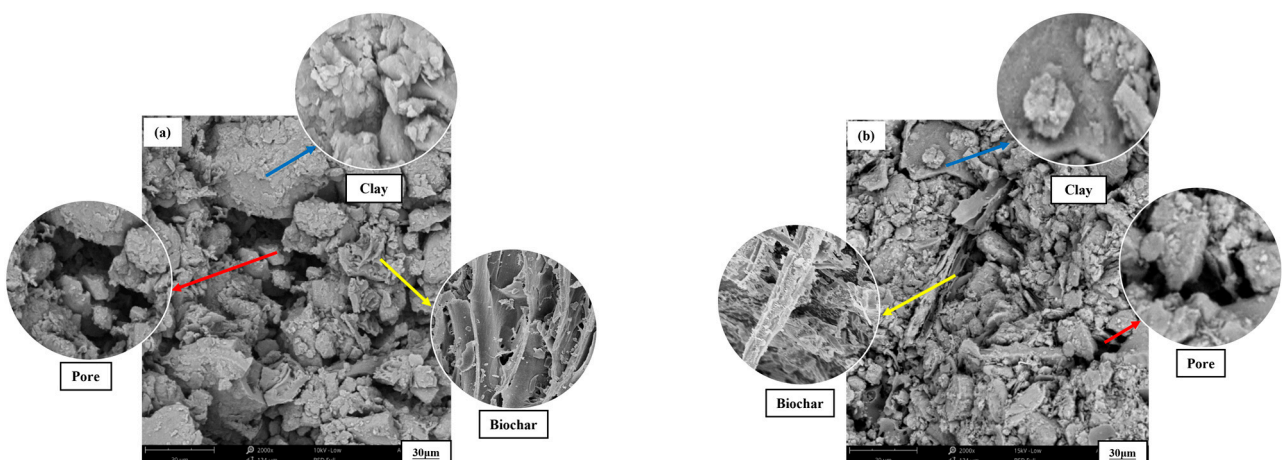


Figure 16. SEM images of the biochar–clay mixture under different biochar contents: (a) $\alpha = 10\%$; (b) $\alpha = 15\%$.

The maximum shear and constrained modulus of the biochar–methanotroph–clay mixture increase with the methane cultivation days. The Poisson’s ratio decreases with the increase in methane cultivation days. By adding biochar-piggybacked methanotrophs to the clay, the growth and reproduction of methanotrophs will impact the macroscopic properties of the soil. Fourier-transform infrared spectroscopy (FTIR) was used to analyze the macroscopic properties of the soil improved by methanotrophs. Figure 17 shows the variation in the functional groups of the biochar–methanotroph–clay mixture ($\alpha = 15\%$), under different methane cultivation days, and the right figure is partially enlarged on the left. Absorption peaks exist at wave numbers of about 1400 cm^{-1} and 1030 cm^{-1} . The absorption peak at about 1400 cm^{-1} is attributed to the $-\text{COO}^-$ symmetric stretching, associated with amino acid-protein species [35,36]. The broad absorption peak at about 1030 cm^{-1} is attributed to the C–O functional group stretching vibrations of polysaccharides [37]. The absorbance of both peaks increases with the increase in methane cultivation days. This indicates that during the process of methane-filled incubation, the methanotrophs produce a large amount of bacterial extracellular polymeric substances (EPS) during the growth in the soil, and the polysaccharides and proteins, which are the main substances of EPS, increase. EPS has strong adsorption and can be well adhered to soil particles or filled between soil particles, reducing the pores inside the soil, so that the maximum shear and constrained modulus tend to increase. EPS also gives cohesion, which enables the soil particles to be tightly connected, enhances the resistance to lateral deformation, and the Poisson’s ratio tends to decrease [38,39].

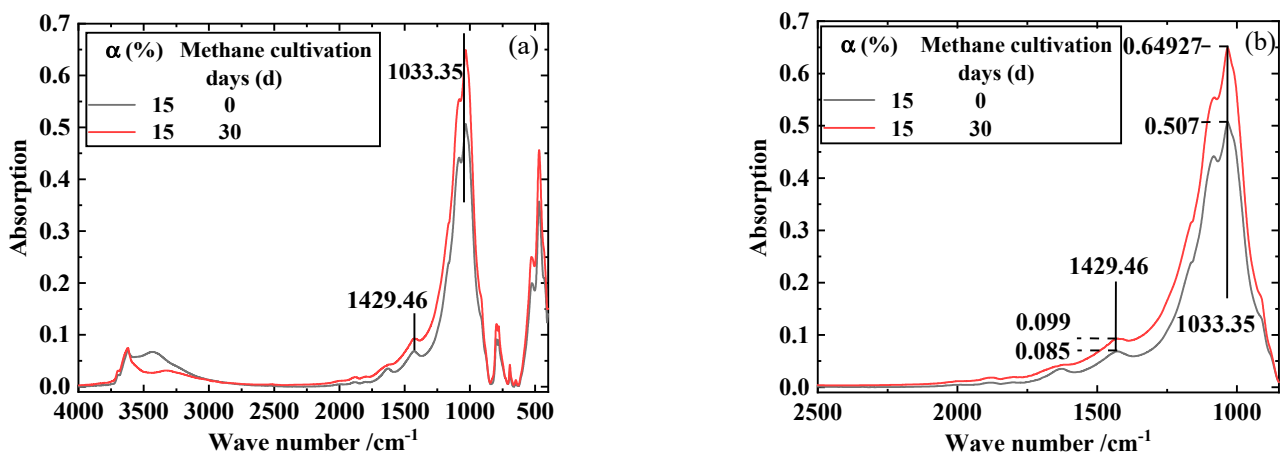


Figure 17. Variation in functional groups of the biochar–methanotroph–clay mixture ($\alpha = 15\%$) under different methane cultivation days: (a) variation in functional groups; (b) enlarged figure.

This study demonstrates that incorporating biochar and methanotrophs in a landfill clay covering layer, can improve the soil structure and enhance the soil integrity, through binder–extender element tests. The effects of the dry density and biochar content on the small-strain elastic parameters (maximum shear modulus, G_{\max} , maximum constrained modulus, M_{\max} , and Poisson’s ratio, ν) of the covering layer soil were also considered, and it was found that G_{\max} and M_{\max} were larger when ρ_d was 1.64 g/cm^3 and α was 15% . Meanwhile, the effects of methanotroph growth on the elastic parameters were considered, to study the long-term service stability of the new covering layer. It was found that methanotrophs produced extracellular polymers, to fill the pores between the mucilages, and the resistance to deformation was enhanced. This study provides a reference for landfill engineering, to form a better design for the covering layer. However, this study did not consider the effects of other factors (e.g., rainfall, temperature change) on the covering layer soil during the service of the landfill, so it is recommended that the influence of other factors be considered in subsequent studies.

5. Conclusions

The maximum shear modulus, G_{\max} , maximum constrained modulus, M_{\max} , and Poisson's ratio, ν , of a biochar–clay mixture and a biochar–methanotroph–clay mixture, were measured by the GDS bender–extender element test. The effects of dry density, biochar content, and methane cultivation days on the small-strain elastic parameters of the biochar–clay mixture and the biochar–methanotroph–clay mixture were analyzed. The main conclusions are as follows:

1. The maximum shear and constrained modulus of the biochar–clay mixture increased with the increase in dry density, and the increasing trend was most obvious when the biochar content was 15%. The maximum shear and constrained modulus of the biochar–clay mixture increased with the increase in biochar content. When the dry density was 1.64 g/cm^3 , the increase in biochar content significantly increased the maximum shear and constrained modulus.
2. The maximum shear and constrained modulus of the biochar–methanotroph–clay mixture increased with the increase in methane cultivation days, and the higher the biochar content, the more obvious the increasing trend of the maximum shear and constrained modulus.
3. The Poisson's ratio of the biochar–clay mixture tended to increase with the increase in dry density and biochar content, and the Poisson's ratio increased obviously when the dry density and biochar content was higher. The Poisson's ratio of the biochar–methanotroph–clay mixture decreased with the increase in methane cultivation days.

Author Contributions: Conceptualization, S.Z. and W.S.; methodology, S.Z. and K.X.; formal analysis, S.Z. and D.L.; investigation, S.Z.; resources, S.Z. and W.S.; data curation, S.Z., K.X. and D.L.; writing—original draft preparation, S.Z. and D.L.; writing—review and editing, W.S. and K.X. All authors have read and agreed to the published version of the manuscript.

Funding: This research was funded by the National Natural Science Foundation of China (Grant number 41977214).

Data Availability Statement: Not applicable.

Acknowledgments: The authors thank the National Natural Science Foundation of China (Grant number 41977214), Shanghai University and Donghua University.

Conflicts of Interest: The authors declare no conflict of interest.

References

1. Alheji, A.K.B.; Yu, J.; Wu, Y.T. Method of dynamic index system for classification and treatment of municipal domestic waste. *J. Civil Environ. Eng.* **2020**, *42*, 153–160.
2. Pachauri, R.K.; Allen, M.R.; Barros, V.R.; Broome, J.; Cramer, W.; Christ, R.; Church, J.A.; Clarke, L.; Dahe, Q.; Dasgupta, P.; et al. Climate Change 2014: Synthesis Report. Contribution of Working Groups I, II and III to the Fifth Assessment Report of the Intergovernmental Panel on Climate Change. *J. Roman. Stud.* **2014**, *4*, 85–88.
3. Reddy, K.; Yaghoubi, P.; Yukselen-Aksoy, Y. Effects of biochar amendment on geotechnical properties of landfill cover soil. *Waste Manag. Res. J. Sustain. Circ. Econ.* **2015**, *33*, 524–532. [[CrossRef](#)]
4. Wu, B.; Xi, B.; He, X.; Sun, X.; Li, Q.; Ouhe, Q.; Zhang, H.; Xue, C. Methane Emission Reduction Enhanced by Hydrophobic Biochar-Modified Soil Cover. *Processes* **2020**, *8*, 162. [[CrossRef](#)]
5. Brindha, R.K.; Vasudevan, N. Methane oxidation capacity of methanotrophs isolated from different soil ecosystems. *Int. J. Environ. Sci. Technol.* **2017**, *15*, 1931–1940. [[CrossRef](#)]
6. Sadasivam, B.Y.; Reddy, K.R. Landfill methane oxidation in soil and bio-based cover systems: A review. *Rev Environ. Sci. Biotechnol.* **2014**, *13*, 79–107. [[CrossRef](#)]
7. Nikbakht, M.; Sarand, F.B.; Irani, A.E.; Bonab, M.H.; Azarafza, M.; Derakhshani, R. An Experimental Study for Swelling Effect on Repairing of Cracks in Fine-Grained Clayey Soils. *Appl. Sci.* **2022**, *12*, 8596. [[CrossRef](#)]
8. Lu, S.G.; Sun, F.F.; Zong, Y.T. Effect of rice husk biochar and coal fly ash on some physical properties of expansive clayey soil (Vertisol). *Catena* **2014**, *114*, 37–44. [[CrossRef](#)]

9. Saffari, R.; Habibagahi, G.; Nikooee, E.; Niazi, A. Biological Stabilization of a Swelling Fine-Grained Soil: The Role of Microstructural Changes in the Shear Behavior. *Iran. J. Sci. Technol. Trans. Civ. Eng.* **2017**, *41*, 405–414. [[CrossRef](#)]
10. Xue, Q.; Zhao, Y.; Li, Z.Z.; Liu, L. Numerical simulation on the cracking and failure law of compacted clay lining in landfill closure cover system. *Int. J. Numer. Anal. Meth. Geomech.* **2014**, *38*, 1556–1584. [[CrossRef](#)]
11. Yang, J.; Yan, X.R. Site response to multi-directional earthquake loading: A practical procedure. *Soil Dyn. Earthq. Eng.* **2009**, *29*, 710–721. [[CrossRef](#)]
12. Lu, N.; Kaya, M. A Power Law for Elastic Moduli of Unsaturated Soil. *J. Geotech. Geoenviron. Eng.* **2013**, *140*, 46–56. [[CrossRef](#)]
13. Zhang, F.; Yang, Z.J.; Still, B.; Wang, J.; Yu, H.; Zubeck, H.; Petersen, T.; Aleshire, L. Elastic properties of saline permafrost during thawing by bender elements and bending disks. *Cold Reg. Sci. Technol.* **2018**, *146*, 60–71. [[CrossRef](#)]
14. Shirley, D.J.; Hampton, L.D. Shear-wave measurements in laboratory sediments. *J. Acoust. Soc. Am.* **1978**, *63*, 607–613. [[CrossRef](#)]
15. Rozova, O.N.; Mustakhimov, I.I.; But, S.Y.; Reshetnikov, A.S.; Khmelenina, V.N. Role of the malic enzyme in metabolism of the halotolerant methanotroph *Methylobacterium alcaliphilum* 20Z. *PLoS ONE* **2019**, *14*, e0225054. [[CrossRef](#)]
16. Teng, H.; Altaf, A.R. Elemental mercury (Hg⁰) emission, hazards, and control: A brief review. *J. Hazard. Mater. Adv.* **2022**, *5*, 100049. [[CrossRef](#)]
17. Altaf, A.R.; Adewuyi, Y.G.; Teng, H.; Gang, L.; Abid, F. Elemental mercury (Hg⁰) removal from coal syngas using magnetic tea-biochar: Experimental and theoretical insights. *J. Environ. Sci.* **2022**, *122*, 150–161. [[CrossRef](#)]
18. Xu, K.; Sun, W.J.; Liu, X.Y.; Yu, C. Methane Reduction Efficiency of Biochar-methanotroph-amended Clay. *Arab. J. Geosci.* **2022**, *15*, 909. [[CrossRef](#)]
19. Gu, X.Q.; Yang, J.; Huang, M.S. Laboratory measurements of small strain properties of dry sands by bender element. *Soils Found.* **2013**, *53*, 735–745. [[CrossRef](#)]
20. Gluchowski, A.; Skutnik, Z.; Biliniak, M.; Sas, W.; Lo Presti, D. Laboratory Characterization of a Compacted–Unsaturated Silty Sand with Special Attention to Dynamic Behavior. *Appl. Sci.* **2020**, *10*, 2559. [[CrossRef](#)]
21. Liu, X.; Qin, H.; Lan, H.X. On the relationship between soil strength and wave velocities of sandy loess subjected to freeze-thaw cycling. *Soil Dyn. Earthq. Eng.* **2020**, *136*, 106216. [[CrossRef](#)]
22. Ruan, B.; Miao, Y.; Cheng, K.; Yao, E.L. Study on the small strain shear modulus of saturated sand-fines mixtures by bender element test. *Eur. J. Environ. Civ. Eng.* **2021**, *25*, 28–38. [[CrossRef](#)]
23. Gao, W.; Munoz, R.V.; Ren, T.; Ashto, R.W.; Morin, M.; Clark, I.M.; Powlson, D.S.; Whalley, W.R. Effect of microbial activity on penetrometer resistance and elastic modulus of soil at different temperatures. *Eur. J. Soil Sci.* **2017**, *68*, 412–419. [[CrossRef](#)] [[PubMed](#)]
24. GB 50123; Standard for Soil Test Method. Ministry of Water Resources of China: Beijing, China, 2019.
25. ASTM D1762-84; Standard test method for chemical analysis of wood charcoal. ASTM International: West Conshohocken, PA, USA, 2007.
26. Kallistova, A.Y.; Montonen, L.; Jurgens, G.; Münster, U.; Kevbrina, M.V.; Nozhevnikova, A.N. Culturable psychrotolerant methanotrophic bacteria in landfill cover soil. *Microbiology* **2013**, *83*, 109–118. [[CrossRef](#)]
27. Ingale, R.; Patel, A.; Mandal, A. Performance analysis of piezoceramic elements in soil: A review. *Sens. Actuators A-Phys.* **2017**, *262*, 46–63. [[CrossRef](#)]
28. Xu, K.; Gu, X.; Hu, C.; Lu, L. Comparison of small-strain shear modulus and Young’s modulus of dry sand measured by resonant column and bender–extender element. *Can. Geotech. J.* **2020**, *57*, 1745–1753. [[CrossRef](#)]
29. Li, M.Y.; Sun, W.J.; Huang, Q.; Sun, D.A. Soil-water characteristic of biochar-clay mixture in the full suction range. *Rock Soil Mech.* **2022**, *43*, 2717–2725. (In Chinese)
30. Soból, E.; Gabryś, K.; Zabłocka, K.; Šadzevičius, R.; Skominas, R.; Sas, W. Laboratory Studies of Small Strain Stiffness and Modulus Degradation of Warsaw Mineral Cohesive Soils. *Minerals* **2020**, *10*, 1127. [[CrossRef](#)]
31. Keller, L.M.; Seiphooori, A.; Gasser, P.; Lucas, F.; Holzer, L.; Ferrari, A. The pore structure of compacted and partly saturated MX-80 bentonite at different dry densities. *Clays Clay Miner.* **2014**, *62*, 174–187. [[CrossRef](#)]
32. Yang, G.C.; Liu, Y.; Chen, P.P. Simulation Analysis of Temperature Effects on the Shear Behavior of Gassy Sand. *Geofluids* **2022**, *2022*, 5602833. [[CrossRef](#)]
33. Tisdall, J.M.; Nelson, S.E.; Wilkinson, K.G.; Smith, S.E.; McKenzie, B.M. Stabilisation of soil against wind erosion by six saprotrophic fungi. *Soil Biol. Biochem.* **2012**, *50*, 134–141. [[CrossRef](#)]
34. Li, M.Y.; Sun, W.J.; Wang, Y.J.; Sun, D.A.; Tan, Y.Z. Air permeability of biochar-amended clay cover. *Arab. J. Geosci.* **2021**, *14*, 732. [[CrossRef](#)]
35. Omoike, A.; Chorover, J. Spectroscopic study of extracellular polymeric substances from *Bacillus subtilis*: Aqueous chemistry and adsorption effects. *Biomacromolecules* **2004**, *5*, 1219–1230. [[CrossRef](#)]
36. Badireddy, A.R.; Korpol, B.R.; Chellam, S.; Gassman, P.L.; Engelhard, M.H.; Lea, A.S.; Rosso, K.M. Spectroscopic characterization of extracellular polymeric substances from *Escherichia coli* and *Serratia marcescens*: Suppression using sub-inhibitory concentrations of bismuth thiols. *Biomacromolecules* **2008**, *9*, 3079–3089. [[CrossRef](#)]
37. Marc-André, G.; Lafleur, M. From curdland powder to the triple helix gel structure: An attenuated total reflection-infrared study of the gelation process. *Appl. Spectrosc.* **2007**, *61*, 374–378. [[CrossRef](#)]

38. Huang, L.; Jin, Y.N.; Zhou, D.H.; Liu, L.X.; Huang, S.K.; Zhao, Y.Q.; Chen, Y.C. A Review of the Role of Extracellular Polymeric Substances (EPS) in Wastewater Treatment Systems. *Int. J. Environ. Res. Public Health* **2022**, *19*, 12191. [[CrossRef](#)]
39. Tan, X.L.; Zhang, G.P.; Yin, H.; Reed, A.H.; Furukawa, Y. Characterization of particle size and settling velocity of cohesive sediments affected by a neutral exopolymer. *Int. J. Sediment Res.* **2012**, *27*, 473–485. [[CrossRef](#)]

Disclaimer/Publisher’s Note: The statements, opinions and data contained in all publications are solely those of the individual author(s) and contributor(s) and not of MDPI and/or the editor(s). MDPI and/or the editor(s) disclaim responsibility for any injury to people or property resulting from any ideas, methods, instructions or products referred to in the content.